Bulletin of Mathematical Biology (1999) **61**, 651–681
Article No. bulm.1999.0101
Available online at http://www.idealibrary.com on IDEAL®

The Effect of Heterogeneously-distributed RyR Channels on Calcium Dynamics in Cardiac Myocytes

PETER A. SPIRO* AND HANS G. OTHMER†
Department of Mathematics,
University of Utah,
Salt Lake City, UT 84112, U.S.A.

Calcium plays an essential role in excitation-contraction coupling in muscle, and derangements in calcium handling can produce a variety of potentially harmful conditions, especially in cardiac muscle. In cardiac tissue specialized invaginations of the sarcolemma, called T-tubules, penetrate deep into each sarcomere, and depolarization of the SL leads to an influx of calcium through voltage-sensitive channels in the T-tubules that in turn triggers further calcium release from the sarcoplasmic reticulum via ryanodine-sensitive calcium channels. Under certain conditions, such as elevated external Ca^{2+}, cardiac cells can release calcium from the sarcoplasmic reticulum spontaneously, producing a calcium 'spark' and propagating traveling waves of elevated Ca^{2+} concentration, without depolarization of the SL (Wier and Blatter, 1991a, *Cell Calcium* **12**, 241–254; Williams, 1993, *Cell Calcium* **14**, 724–735; Cheng *et al.*, 1993a, *Science* **262**, 740–744). However, under normal resting conditions these potentially harmful waves seldom occur. In this paper we investigate the role of the periodic distribution of ryanodine-sensitive channels in determining whether a spark can trigger a wave, using a modification of the kinetic model proposed by Tang and Othmer, 1994b, *Biophys. J.* **67**, 2223–2235, for calcium-induced calcium release. We show that the spatial localization of these channels near the T-tubules has a significant effect on both wave propagation and the onset of oscillations in this system. Spatial localization provides a possible explanation for the differing effects of various experimental protocols on the system's ability to propagate a traveling wave.

1. INTRODUCTION

Calcium (Ca^{2+}) is a ubiquitous intracellular messenger used to activate a wide variety of cellular processes, including muscle contraction, fertilization and development of deuterostome eggs, cell growth, neuromodulation and synaptic plasticity, and sensory perception (Berridge, 1993). Calcium activates cellular processes by increased binding to key signaling proteins following an increase in cytosolic calcium concentration ($[Ca^{2+}]_i$). The increase in $[Ca^{2+}]_i$ is usually in response to an

*Current address: Incyte Pharmaceuticals Inc., 3174 Porter Drive, Palo Alto, CA 94304, U.S.A.
†Supported in part by NIH Grant GM29123.

0092-8240/99/040651 + 31 $30.00/0

extracellular signal, such as an action potential or the binding of a ligand to a transmembrane receptor. In the latter case this can lead, through a series of chemical steps, to the internal production of inositol trisphosphate (IP_3), which then binds to IP_3 receptors (IP_3 Rs) on the membrane of the endoplasmic reticulum (ER), an internal compartment which stores Ca^{2+} at concentrations much higher than in the cytosol. The IP_3 Rs are Ca^{2+} channels which are opened by the binding of IP_3, generating a gradient-driven flux of Ca^{2+} into the cytosol. Existing models of this process are reviewed in Tang *et al.* (1996).

In cardiac and other muscle cells, the primary role of Ca^{2+} is to mediate excitation-contraction coupling (ECC), the process by which an action potential produces muscle contraction. ECC is initiated by the rapid propagation of an action potential along the cell membrane (the sarcolemma, or SL) and from one cell to another. The action potential propagates both along the surface membrane of the cell, as well as along the transverse tubules (T-tubules), which are invaginations of the SL which extend deep into the cell. In cardiac myocytes the action potential opens voltage-opened channels (VOCs), mostly of the form known as L-type channels, in the SL. This results in an influx of Ca^{2+} because resting $[Ca^{2+}]_i$ is maintained at a lower level ($\sim$0.1 μM) than the extracellular Ca^{2+} concentration ($[Ca^{2+}]_e \sim 1$ mM). The rise in $[Ca^{2+}]_i$ resulting from the Ca^{2+} influx triggers calcium-induced calcium release (CICR) from the sarcoplasmic reticulum (SR), where Ca^{2+} is stored at elevated concentrations. [Free Ca^{2+} concentration in the SR ($[Ca^{2+}]_{sr}$) is, again, about 1 mM, and total $[Ca^{2+}]$ in the SR may be about ten times higher, due to heavy buffering Bers (1991a)]. Released Ca^{2+} then diffuses into the myofibrils — specialized structures containing the actin and myosin filaments — and induces contraction. Whereas extracellular Ca^{2+} provides the trigger, CICR provides the majority of Ca^{2+} used in activating contraction in cardiac muscle (Bers, 1991a; Spencer and Berlin, 1997).

Calcium release from the SR through the ryanodine-sensitive channels (RyRs), which open in response to the initial rise in $[Ca^{2+}]_i$, apparently also involves self-stimulation by released Ca^{2+}. Most of the RyRs are in the terminal cisternae or junctional SR (JSR), the portions of the SR directly abutting the T-tubules. The RyRs are thus located in close apposition to the VOCs, a property which facilitates opening of the RyRs by the Ca^{2+} trigger. The proximity of the RyRs and VOCs suggests the existence of cytosolic Ca^{2+} microdomains (Stern, 1992), in which $[Ca^{2+}]_i$ adjacent to these channels may rise substantially above the cell-averaged $[Ca^{2+}]_i$. However, the release mechanism is not completely understood, and factors other than cytosol Ca^{2+} may be involved. For instance, Ikemoto *et al.* (1992), found that luminal Ca can trigger Ca release from the SR.

The autocatalytic release of Ca^{2+} terminates once $[Ca^{2+}]_i$ reaches a sufficiently high level, probably because opening of the RyRs is inhibited by high Ca^{2+} concentrations (Fabiato, 1985; Schiefer *et al.*, 1995; Laver and Lamb, 1998). The equilibrium response of the channels to Ca^{2+} is thus bell-shaped. Once CICR has ended, processes which take up Ca^{2+} from the cytosol dominate the Ca^{2+} dynamics. These processes involve transport of Ca^{2+} into the extracellular medium and into the

SR by exchangers and pumps located in the SL and the SR membrane (Bers, 1991b). Calcium uptake makes the Ca^{2+} signal a transient 'spike', and allows the cell to maintain very low levels of resting $[Ca^{2+}]_i$.

The response to the triggering event is both excitable and graded. The amount of Ca^{2+} released autocatalytically is considerably greater than the initial influx of Ca^{2+} (Spencer and Berlin, 1997), but only if this initial influx exceeds a threshold level (Othmer and Tang, 1993; Tang and Othmer, 1994a). We refer to this property as excitability. However, channel dynamics are inherently stochastic and the response is not all-or-none. The magnitude of the Ca^{2+} response at the cell level increases with the magnitude of the flux through the VOCs (Beuckelmann and Wier, 1988; Stern, 1992; Tang and Othmer, 1994a), this property is known as gradedness.

In many cell types, calcium signaling exhibits a variety of dynamical behaviors. In addition to the excitable behavior just described, rhythmic oscillations in $[Ca^{2+}]_i$ involving repetitive periods of Ca^{2+} release and uptake, can occur. Self-oscillatory behavior has been reported both in IP_3-mediated signaling (Putney and Bird, 1993) and in muscle cells (Wier and Blatter, 1991b; Fabiato, 1992; Williams, 1993). Many cell types exhibit traveling waves of elevated $[Ca^{2+}]_i$ (Berridge, 1993; Jaffe, 1993; Rooney and Thomas, 1993; Williams, 1993). These waves involve diffusion of locally-released Ca^{2+} to neighboring release sites, causing neighboring channels to open and release more Ca^{2+}, which in turn diffuses. Calcium waves may serve a physiological purpose in some cell types (Allbritton and Meyer, 1993; Rooney and Thomas, 1993).

In cardiac myocytes, the rapid propagation of the action potential normally triggers an excitation response nearly simultaneously throughout the length of a cell, allowing the entire cell to contract at once. Under abnormal conditions, however, the dynamics can be different. Local, spontaneous, oscillatory release of Ca^{2+} can occur occasionally under normal conditions (Stern *et al.*, 1988), and occurs regularly when $[Ca^{2+}]_e$ is raised above 3 mM (Stern *et al.*, 1988), when $[Ca^{2+}]_i$ is raised in a 'skinned' cell from which the SL has been removed (Wier and Blatter, 1991b; Fabiato, 1992), and possibly at locations of cell damage (Williams, 1993). Traveling Ca^{2+} waves can propagate throughout a portion or the entire length of a cell. Waves can be initiated from sites of oscillatory Ca^{2+} release (Stern *et al.*, 1988) or by a transient local release of Ca^{2+} (a Ca^{2+} 'spark') under conditions of elevated ($\geq$ 10 mM) $[Ca^{2+}]_e$ (Cheng *et al.*, 1996a, b). Wave propagation occurs in most cardiac myocytes at elevated $[Ca^{2+}]_e$ but seldom occurs at normal physiological (1 mM) $[Ca^{2+}]_e$ (Cheng *et al.*, 1996a). Calcium wave propagation in cardiac tissue is accompanied by arrhythmogenic membrane currents and so may be potentially dangerous (Wier and Blatter, 1991b).

It has recently been found that calcium signaling also exhibits subcellular spatial heterogeneity. Both RyRs and IP_3 Rs tend to be localized in nodes or clusters, separated by regions of low channel density. These nodes spontaneously release Ca^{2+} in quanta referred to as 'sparks' or 'puffs', which are believed to constitute fundamental units of Ca^{2+} release. Such 'quantal release' has been reported in a

wide range of Ca^{2+} signaling systems, including in IP_3-mediated signaling (Parker and Yao, 1991; Parker and Ivorra, 1993; Parker and Yao, 1995; Parys *et al.*, 1996); in cardiac tissue (Cheng *et al.*, 1993b; López-López *et al.*, 1994; Lipp and Niggli, 1994; Taylor, 1994; López-López *et al.*, 1995; Niggli and Lipp, 1995; Shacklock *et al.*, 1995; Wier *et al.*, 1995; Lipp and Niggli, 1996), skeletal (Monck *et al.*, 1994; Tsugorka *et al.*, 1995), and in smooth muscle (Fay, 1995; Nelson *et al.*, 1995); and by RyRs in nonmuscle cells (Cheek *et al.*, 1994; Monck *et al.*, 1994). Calcium waves are believed to be composed of series of sequentially-recruited sparks or puffs, a property sometimes reflected by a wave having a saltatory appearance, particularly when the system is near a wave propagation threshold (Cheng *et al.*, 1996a, b; Parker and Yao, 1991; Parker *et al.*, 1996b). Our focus here is on the effect of the nonuniformity of Ca^{2+} channel distribution on the dynamics of Ca^{2+} signaling, particularly on the propagation of Ca^{2+} waves.

Spatial heterogeneity in cardiac myocytes has many aspects, but here we are concerned only with those related to calcium handling. In striated muscle the myocyte is roughly cylindrical and consists of longitudinally-repeated units called sarcomeres, each of which comprises a central A band of thick fibers and two half I bands of thin fibers at each end, terminated by Z bands (Katz, 1992). T-tubules and the majority of the RyRs are located at the endpoints of sarcomeres, and so have a periodic distribution of period equal to the sarcomere length (about 1.9 μm). T-tubules constitute a large fraction of the SL (Bers, 1991b), and because the cells are quite thick [14–20 μm (Jaffe, 1993)], the nearest SL at most points within the myofibrils is at a T-tubule, rather than the external surface of the cell. Therefore, since VOCs are located in the SL, the major sites of Ca^{2+} entry through the SL have a periodic distribution of the same period as the T-tubule spacing. Sites of calcium release from the SR have a similar distribution, due to the proximity of JSR to the SL.

The periodic distribution of Ca^{2+} channels is reflected in the dynamical behavior of cardiac Ca^{2+} signaling. Both spontaneous Ca^{2+} sparking and normal release of Ca^{2+} during ECC have a heterogeneous distribution (Cannell *et al.*, 1994; Cheng *et al.*, 1996a), and both tend to occur at the junctions between T-tubules and the SR (Cheng *et al.*, 1996b; Tanaka *et al.*, 1998). In addition, wave propagation appears to consist of sequential recruitment of Ca^{2+} sparks, centered at these junctions, and so progresses in a saltatory manner (Cheng *et al.*, 1996a; Keizer *et al.*, 1998; Keizer and Smith, 1998). The nonuniformity in wave propagation is particularly pronounced at low wave speeds, though this has been attributed to poor experimental resolution of faster waves (Cheng *et al.*, 1996a). These recent findings suggest the need for a theoretical analysis of the extent to which various features of cardiac Ca^{2+} dynamics are determined by spatial heterogeneity.

Most modeling of calcium dynamics has been done for IP_3-mediated signaling [reviewed in Dupont and Goldbeter (1992); Keizer *et al.* (1995); Li *et al.* (1995); Tang *et al.* (1996)]. Less has been done for cardiac Ca^{2+} dynamics. There exist several mechanistic models of RyR dynamics, involving binding of Ca^{2+} to both excitatory and inhibitory sites. A detailed model involving cooperative Ca^{2+} binding

and interactions among monomers of the RyR tetramer has been used to explain channel adaptation (Cheng *et al.*, 1995). RyR adaptation is also reproduced in the four-state model of Keizer and Levine (1996). However, in Tang and Othmer (1994a) it is shown that a simple four-state 'adapting box' model is sufficient to reproduce adaptation [see also Sachs *et al.* (1995)]. The model of Tang and Othmer (1994b) is probably the most complete model of Ca^{2+}-handling in cardiac myocytes [since the more detailed model of Cheng *et al.* (1995) addresses only RyR dynamics]. It reproduces CICR, excitability, graded response, and spontaneous oscillations at elevated $[Ca^{2+}]_i$.

To our knowledge, the effect of heterogeneity on cardiac Ca^{2+} dynamics has not been addressed previously in a mechanistic model. We do this below, and we begin in Section 2 by applying analytical results on heterogeneity in reaction–diffusion systems to show that this effect can be expected to be significant. In Section 3 we present a model for Ca^{2+} cardiac dynamics which incorporates heterogeneous signaling, and in Section 4 we present numerical simulations of the model in which we examine the effect of the heterogeneity. We find significant effects due to heterogeneity, particularly on the capacity of the system to propagate traveling waves and on the threshold for onset of self-oscillatory behavior. We show that if heterogeneity is present, there exist physiologically-reasonable parameter sets which lie near 'bifurcation' points for traveling wave-blocking. By this we mean that a moderate change in a parameter (for example a rise in external $[Ca^{2+}]$) can move the system from a wave-blocking to a wave-propagating regime. The significance of these findings is discussed in Section 5.

2. General Considerations on Heterogeneity of Sources in Reaction–diffusion Systems

Consider a general reaction–diffusion system of the form

$$\frac{\partial u}{\partial t} = \mathcal{D}\Delta u + f(u), \tag{1}$$

where u is a vector of state variables, $\mathcal{D}$ is a matrix of diffusion coefficients, and $f(u)$ is a nonlinear 'reaction' term. In the present context of Ca^{2+} dynamics u could comprise the Ca^{2+} concentration in the cytosol, the extracellular space and in the ER, the channel states, complexes of Ca^{2+} with buffers, etc. A complete model is given in the following section. A considerable amount of work has been done on the effects of heterogeneity on the dynamics of reaction–diffusion systems. However, most analyses have focused on the effect of heterogeneous diffusion. These include models of diffusively coupled cells (Othmer, 1983; Neu and Krassowska, 1993), myelinated axon conduction [see Bell (1990) for a review], patchy environments in ecology (Shigesada *et al.*, 1985, 1986) and flame propagation (Xin and Zhu, 1995). In Othmer (1983), stable, stationary solutions are constructed in a system of coupled

cells using bistable kinetics, and the existence of such solutions precludes traveling fronts in these systems. Comparatively little work has been done on the effect of spatially-variable reaction terms, and few theoretical results have been established. In Spiro (1997), we investigate the effect of spatially-periodic reaction terms on the behavior of such systems in detail, but here, we use some of the results without giving the analytical justification. On the basis of scaling arguments, one expects that whether or not the periodic arrangement of the local dynamics is important depends on whether the characteristic time for diffusion of the important species over one spatial period is small or large compared to a characteristic time for the local dynamics. The former is measured by $\tau_d \equiv L^2/D$, where L is the period of the spatial heterogeneity and D is an effective diffusion coefficient, while the latter is designated τ_r, and must be estimated from the local dynamics embodied in $f(u)$. When the parameter $\theta \equiv \tau_d/\tau_r$ is much less than unity, diffusion is fast compared to the local dynamics, and the analysis shows that the effect of heterogeneity will be insignificant. However, when θ is of order one or larger, the presence of heterogeneity can significantly affect the system's dynamics. In the following paragraphs we estimate θ for the cardiac context and find that it is not small, so that the effect of heterogeneity on the system's dynamics will be significant. To estimate θ we must estimate the physiological length scales of the heterogeneity (L) and the characteristic time scales for diffusion and the local dynamics. Estimates of L and D are at hand, and to estimate the time scale τ_r we proceed as follows.

The primary issue in this paper is whether or not long-range propagation can be initiated and sustained by localized release of Ca^{2+}, and this should depend on a competition between the effect of diffusion, which provides the mechanism for coupling the release sites, and the effect of the reaction terms in areas of low $[Ca^{2+}]_i$ — in particular, the mechanisms for Ca^{2+} removal from the cytosol — which can quench the leading edge of a propagating signal by re-sequestering the $[Ca^{2+}]_i$. Whether (and how fast) a signal propagates should depend on how much Ca^{2+} can diffuse to an area of low concentration before the reaction processes in this area can remove the Ca^{2+}. The time scale τ_r should, therefore, reflect the time scale of excitation at the steady state.

The time scale of excitation, which reflects a competition between Ca^{2+} release and uptake, is difficult to estimate from experimental data, particularly since the properties of the main removal mechanism, the SR pump, have not been accurately measured (Bers, 1991b). We therefore estimate it from the reaction term dynamics of a theoretical model of the system. To understand how to estimate τ_r in this manner we first consider the single variable bistable system, for which $f(u) = u(u-a)(1-u)$. For this system, the exponential time constant which measures the time scale for decay of small perturbations is the slope of the reaction term f at the steady state,

$$\tau_r = -1/f'(0). \tag{2}$$

For a model of Ca^{2+} signaling, which necessarily involves a multidimensional state variable vector u and a multidimensional reaction term f, we consider the multidimensional analog of equation (2). We find the eigenvalues λ_i and eigenvectors v_i, $i = 1, 2, \ldots$, of the Jacobian of f at the spatially uniform steady state u_{SS} from the equation

$$D_u f(u_{SS}) v_i = \lambda_i v_i. \tag{3}$$

To obtain a unique time scale for excitation, we assume that exactly one of the eigenvectors, v_e, will correspond to the direction of excitation/decay in state space, and that the corresponding eigenvalue λ_e then gives the rate of decay to steady state,

$$\tau_r = -1/\lambda_e. \tag{4}$$

We apply this procedure to existing models of calcium signaling, in both cardiac myocytes [using the model of Tang and Othmer (1994a); see Section 3] and IP_3-mediated signaling [using the model of Othmer and Tang (1993)]. For each model we numerically calculate the spatially-uniform, steady-state solution u_{SS} and then the Jacobian $D_u f(u_{SS})$. We then examine each eigenvector to determine which corresponds to the direction of excitation, which we define by the requirements that the elements of v corresponding to $[Ca^{2+}]_i$ and $[Ca^{2+}]_{sr}$ (or $[Ca^{2+}]_{er}$) having opposite sign (indicating release of Ca^{2+} from the SR into the cytoplasm) and that the elements corresponding to $[Ca^{2+}]_i$ and open channel fraction have the same sign (indicating opening of the channels). We find that exactly one eigenvector satisfies these conditions in both models.

The results of these calculations are summarized in Table 1. They reveal that the scaling parameter θ is greater than 1 for both of these systems, and thus we should expect a significant effect of heterogeneity on the systems' dynamics. We explore this possibility in a model for cardiac-calcium signaling in the following sections[†].

3. A Model of Cardiac Calcium Signaling

The model describes Ca^{2+} diffusion within both the cytoplasm and the SR, and Ca^{2+} transport across both the SL and SR membranes. For each membrane, the transport processes consist of a Ca^{2+} channel release term, a Ca^{2+} removal

[†]There is wide variability in the range of diffusion coefficients reported in the literature. For instance Parker *et al.* (1996a), report a value of 17 $\mu m^2\ s^{-1}$ in *Xenopus* oocytes. The 400 $\mu m^2\ s^{-1}$ used here for the cardiac estimate and later, is near the upper end of the reported values (cf. Table 2). To date, there is no accepted *in vivo* value, but as will be seen later, using a diffusion coefficient at the upper end of the range leads to conservative estimates in the context of the questions we address. A smaller diffusion coefficient will only steepen the spatial nonuniformity we report later. For the same reason we do not explicitly account for buffering, since that only reduces the diffusion coefficient.

Table 1. Estimates of parameter values for calcium signaling.

	Cardiac	IP_3
L	1.9 μm[a]	6 μm[b]
D	400 $\mu m^2\ s^{-1}$[a]	500 $\mu m^2\ s^{-1}$[c]
τ_d	9 ms	72 ms
Model	Tang and Othmer (1994a)	Othmer and Tang (1993)[d]
τ_r	1.3 ms	26 ms
θ	7	2.76

[a]Cheng *et al.* (1996a). [b]Parker and Yao (1995). [c]Othmer and Tang (1993). [d]For this model's $[IP_3]$ parameter, we have used a concentration of 366 nM, the level at which the system becomes self-oscillatory (Othmer and Tang, 1993). For lower $[IP_3]$ levels, θ has a somewhat higher value. Because θ is greater than 1 even at the onset of oscillations, we would expect the effect of heterogeneity to be significant over a wide range of $[IP_3]$ levels.

term, and a leakage term. For the SR, the Ca^{2+} release term represents release through the RyRs, and Ca^{2+} uptake represents the action of the SR pump. The sarcolemma Ca^{2+} removal term represents the action of the Na^+/Ca^{2+} exchanger. [In cardiac myocytes, the flux through the SL pump — the other sarcolemma Ca^{2+} removal mechanism — is comparatively insignificant (Bers, 1991b).] The SL channel term, which represents release through the L-type channels, is modeled as a forcing parameter; its dynamics are not an integral part of the present model.

The Ca^{2+} removal terms are modeled using Michaelis–Menten kinetics. The pump term incorporates cooperativity in Ca^{2+} binding, with a Hill coefficient of 2. The RyR channel and leakage terms are proportional to the Ca^{2+} concentration difference between the SR and cytoplasm. The RyR channel term is also proportional to the fraction of channels in the open state. We assume that Ca^{2+} can bind independently to both an excitatory site on the RyR which causes the channel to open, and to an inhibitory site which closes the channel. We neglect the possibility of cooperativity among RyRs. This results in the following four-state model of channel state transitions [cf. Tang and Othmer (1994a)],

$$\begin{array}{ccc} R & \underset{l_{-1}}{\overset{l_1}{\rightleftharpoons}} & RC^+ \\ {\scriptstyle l_{-2}}\uparrow\downarrow{\scriptstyle l_2} & & {\scriptstyle l_{-2}}\uparrow\downarrow{\scriptstyle l_2} \\ RC^- & \underset{l_{-1}}{\overset{l_1}{\rightleftharpoons}} & RC^+C^- \ . \end{array} \tag{5}$$

Here R represents the RyR, C^+ represents Ca^{2+} bound to the excitatory site and C^- represents Ca^{2+} bound to the inhibitory site. There is a single state, RC^+, in which the channel is open.

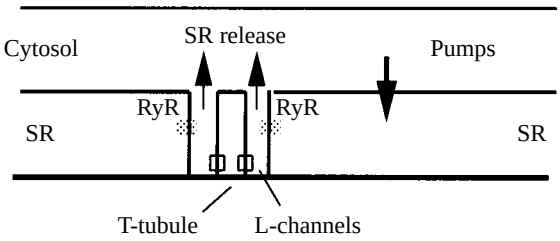

Figure 1. A schematic of the major components in the one-dimensional model. The calcium in both the cytosol and the SR is uniform at any cross-section, and exchange between the two phases occurs due to release from the SR and re-uptake via the pumps. Not shown are the SR leak and the SL transport. The entire structure at the T-tubules is repeated periodically in the x-direction.

We restrict the model to one spatial dimension, in the direction of the longitudinal axis of the cell, and explicitly incorporate spatial heterogeneity into the Ca^{2+} dynamics (cf. Fig. 1). The SL transport terms and the RyRs are given a periodic step-function spatial distribution corresponding to the distribution of T-tubules. It is known that the SR pumps are distributed relatively evenly throughout both the JSR and the remainder of the SR [the free SR, or FSR: (Bers, 1991b)]; thus, we suppose that the SR pump and leak terms are distributed uniformly. Diffusion of Ca^{2+} within the SR is restricted in the sense that we impose no-flux boundary conditions in the SR at the midpoint of each T-tubule location. We also impose no-flux boundary conditions at the endpoints of the entire domain of both the cytoplasm and SR domains, but there are no barriers to diffusion within the cytoplasm. Diffusion coefficients for both domains are constant in space, although in reality various subcellular structures presumably cause variability in diffusion rates.

The model contains five state variables, $u_1, \ldots, u_5$. The variables u_1, u_2, and u_3 are channel state variables, representing the fractions of channels in the R, RC^+, and RC^+C^- states, respectively. The fraction in the fourth state, RC^-, is given by the conservation condition on total channels as $1-u_1-u_2-u_3$. The two remaining state variables, u_4 and u_5, represent the Ca^{2+} concentration in the cytoplasm and SR, respectively. The model equations consist of ordinary differential equations for the channel state transitions,

$$\frac{du_1}{dt} = -(l_1 + l_2)u_4u_1 + l_{-1}u_2 + l_{-2}(1 - u_1 - u_2 - u_3) \tag{6}$$

$$\frac{du_2}{dt} = l_1u_4u_1 - l_{-1}u_2 - l_2u_4u_2 + l_{-2}u_3 \tag{7}$$

$$\frac{du_3}{dt} = l_1u_4(1 - u_1 - u_2 - u_3) + l_2u_4u_2 - (l_{-1} + l_{-2})u_3, \tag{8}$$

and partial differential equations for diffusion and exchange of calcium,

$$\frac{\partial u_4}{\partial t} = D_c \frac{\partial^2 u_4}{\partial x^2} + \left[\underbrace{J(x,t)}_{\text{SL channel flux}} - \underbrace{\frac{q_1 u_4^m}{u_4^m + q_2^m}}_{\text{SL extrusion}} + \underbrace{s_2([\text{Ca}^{2+}]_e - u_4)}_{\text{SL leak}} \right] g(x)$$

$$+ v_r \left[\underbrace{ch \cdot u_2(u_5 - u_4)g(x)}_{\text{SR channel flux}} - \underbrace{\frac{p_1 u_4^2}{u_4^2 + p_2^2}}_{\text{SR pump}} + \underbrace{s_1(u_5 - u_4)}_{\text{SR leak}} \right] \tag{9}$$

$$\frac{\partial u_5}{\partial t} = D_{sr} \frac{\partial^2 u_5}{\partial x^2} - ch \cdot u_2(u_5 - u_4)g(x) + \frac{p_1 u_4^2}{u_4^2 + p_2^2} - s_1(u_5 - u_4). \tag{10}$$

Heterogeneity in the reaction terms is provided by the periodic step-function distribution $g(x)$, with period equal to the sarcomere length L and step width equal to the width δ of the T-tubules. In order to make use of measurements expressed as cell averaged values, we normalize g to have unit average value,

$$g(x) = \begin{cases} L/\delta, & nL \le x < nL + \delta \\ 0, & nL + \delta \le x < (n+1)L \end{cases} . \tag{11}$$

Values and brief descriptions of the model parameters are given in Table 2.

This model is derived from the Tang–Othmer model (Tang and Othmer, 1994a), which has the same form as equations (6)–(10), but from which the present model differs in several respects. Most significant for our purpose here is that the Tang–Othmer model incorporates neither spatial heterogeneity ($g(x) \equiv 1$) nor diffusion within the SR ($D_{sr} = 0$). Furthermore, this model does not reproduce all of the important behaviors. Its dynamics become oscillatory at $[\text{Ca}^{2+}]_e$ levels not far above physiological levels, and at $[\text{Ca}^{2+}]_e = 10$ mM the system is no longer responsive to external stimuli. Thus, it cannot reproduce the recent finding of Cheng *et al.* (1996a), that, raising $[\text{Ca}^{2+}]_e$ to near this level allows propagation of a Ca^{2+} signal in cardiac myocytes, nor does it capture the recent finding (Valdivia *et al.*, 1995) that under physiological conditions (in particular, physiological $[\text{Mg}^{2+}]$), RyR adaptation is considerably faster (~100 ms) than the slower rate (~1 s) obtained in the absence of Mg^{2+} (Gyorke and Fill, 1993; Vélez *et al.*, 1997). The present model reproduces these features, and has also been improved by taking into account recent experimental measurements of a number of system parameters.

4. Numerical Results

The present model reproduces a variety of behaviors seen in experiment. These include a bell-shaped channel open probability function, correct time scales for

Table 2. Parameter definitions and values for the present model, and comparison to values from the literature.

Symbol	Value used	Literature value	Definition
D_c	400 $\mu m^2\ s^{-1}$	100–500 $\mu m^2\ s^{-1}$ [a]	Cytosolic diffusion coefficient
D_{sr}	400 $\mu m^2\ s^{-1}$	100–500 $\mu m^2\ s^{-1}$ [b]	SR diffusion coefficient
L	2 μm	1.9 μm [c]	Period of heterogeneity
δ	0.2 μm	0.2 μm [d]	Width of T-tubules
v_r	0.036	0.036 [e]	SR/cytoplasm volume ratio
m	1	1 [f]	Ca^{2+} extrusion Hill coefficient
q_1	500 $\mu M\ s^{-1}$	150 $\mu M\ s^{-1}$ [g]	Ca^{2+} extrusion V_{max}
q_2	6 μM [h]	1 μM [i]	Ca^{2+} extrusion K_m
s_2	$8.2 \times 10^{-3}\ s^{-1}$ [j]	NA [k]	SL leakage rate
l_1	$20(\mu M \cdot s)^{-1}$ [l]		Excitatory Ca^{2+} binding rate
l_{-1}	80 s^{-1} [l]		Excitatory Ca^{2+} dissociation rate
l_2	$2.7(\mu M \cdot s)^{-1}$ [l]		Inhibitory Ca^{2+} binding rate
l_{-2}	1.5 s^{-1}	1.5 s^{-1} [m]	Inhibitory Ca^{2+} dissociation rate
ch	100 s^{-1}	117 s^{-1} [n]	RyR conductance
p_1	6638 $\mu M\ s^{-1}$	7000 $\mu M\ s^{-1}$ [o]	SR pump V_{max}
p_2	0.15 μM [p]	0.2–5 μM [q]	SR pump K_m
s_1	$2.04 \times 10^{-3}\ s^{-1}$	NA [r]	SR leakage rate
C_0	1000 μM	1000 μM [s]	Normal external Ca^{2+} concentration
J			Ca^{2+} flux through VOCs

[a]Peskoff (1992); Jaffe (1993); Dupont and Goldbeter (1994); Cheng *et al.* (1996a). [b]Ca^{2+} diffuses in the SR at a rate similar to that of the cytoplasm (Bers, 1991b). [c]Cheng *et al.* (1996a). [d]Bers (1991b). [e]Rat ventricle FSR and JSR occupy 3.15% and 0.35% of cell volume, respectively (Bers, 1991b; Katz, 1992), so total SR occupies 3.5%. Since the JSR/FSR volume ratio, 1/9, is equal to the ratio $\delta/(L-\delta)$ of the lengths of the T-tubular and inter-T-tubular regions, and since JSR is located at the T-tubules (Bers, 1991b; Katz, 1992), we use a spatially uniform volume ratio. [f]The Na^+/Ca^{2+} exchanger exchanges 1 Ca^{2+} ion for 3 Na^+ ions and is the predominant pathway for Ca^{2+} extrusion in cardiac myocytes (Bers, 1991b). [g]Bers (1991b). The resulting rate of Ca^{2+} extrusion at rest, $q_1 u_4/(u_4+q_2) = 150 \times 0.1/(0.1+1) = 13.6\ \mu M\ s^{-1}$ (using a resting $[Ca^{2+}]_i$ level $u_4 = 0.1\ \mu$M), is comparable to that of the model, $500 \times 0.1/(0.1+6) = 8.2\ \mu M\ s^{-1}$. [h]Lower values of q_2 prevent the model from exhibiting the observed excitation response at elevated $[Ca^{2+}]_e$ (Cheng *et al.*, 1996a), because as $[Ca^{2+}]_e$ is raised, resting $[Ca^{2+}]_i$ soon exceeds the level at which the RyRs are maximally open. Inclusion of explicit microdomains (Stern, 1992) would allow a lower q_2 (see discussion in Section 4.3). [i]Bers (1991b). [j]Chosen to yield a physiological resting $[Ca^{2+}]_i$ level ($\sim$0.1 μM) at physiological $[Ca^{2+}]_e$ (1 mM). [k]No reliable estimate is available (Bers, 1991b). [l]Chosen to make RyRs maximally open at $[Ca^{2+}]_i$ in the 1–10 μM range (Fabiato, 1985) and to reproduce RyR channel opening and adaptation times of $<$10 ms and 100 ms, respectively, to a step increase in $[Ca^{2+}]_i$ from 0.1 to 1 μM in the presence of physiological $[Mg^{2+}]$ (Valdivia *et al.*, 1995). [m]The time scale of channel inactivation is $\sim$0.7 s (Fabiato, 1985). [n]RyR channel density of 36 nM (Bers, 1991b) and an individual channel conductance of 2 pA for an SR-cytoplasm Ca^{2+} concentration difference of 53 mM (Rousseau *et al.*, 1986) yields a conductance rate constant $v_r \cdot ch \sim eq 4.2\ s^{-1}$. [o]$v_r \cdot p_1 = 250\ \mu M\ s^{-1}$, although this has not been reliably measured *in vivo* (Bers, 1991b). [p]Chosen to yield a physiological resting level ($\sim$1 mM) for $[Ca^{2+}]_{sr}$ (Bers, 1991b). [q]The pump has a K_m of 1–5 μM in isolation, a value that can be decreased 3- to 5-fold through phosphorylation by phospholamban, but *in vivo* measurements are not available (Bers, 1991b). [r]No reliable estimate is available (Bers, 1991b). [s]Bers (1991b).

channel excitation and adaptation, correct resting [Ca^{2+}] levels, excitability, graded response, spontaneous oscillations under perturbed conditions, wave blocking at physiological $[Ca^{2+}]_e$, and wave propagation at higher $[Ca^{2+}]_e$. These behaviors are illustrated below. In addition, we show that the wave propagation behavior of the model depends strongly on the spatial distribution of Ca^{2+}-handling mechanisms. We, furthermore, show that with heterogeneity present, our physiologically-reasonable parameter set lies near a 'bifurcation' point for traveling wave-blocking, meaning that a moderate change in a parameter (such as a rise in external $[Ca^{2+}]$) can move the system from a wave-blocking to a wave-propagating regime.

4.1. ***Numerical methods.*** The results presented below are from numerical simulations of the system of ordinary differential equations (6)–(8) for the channel state transitions (Section 4.2) and for the full system of partial differential equations (6)–(10) (subsequent sections). The LSODE package (Hindmarsh, 1983) for solution of systems of ordinary differential equations was used in the simulations of channel state transitions. For the full reaction–diffusion system we have used a semi-implicit solution method, namely a backward Euler scheme for the diffusion term and a forward Euler scheme for the reaction term.

In the full reaction–diffusion system, no-flux boundary conditions, using a ghost point, are imposed at the end points of the domain, as well as between sarcomeres (once per every length L) for diffusion of Ca^{2+} within the SR. We use a time step $\Delta t = 1\ \mu$s to ensure resolution on the fastest time scale of the system, that of the RyRs, which can be as fast as 1×10^{-5} s. We find that time steps much larger than this can lead to significant numerical error, while decreasing the time step below this value does not change the solutions to the system. We use the largest possible grid spacing, $\Delta x = 100$ nm, which is half the width δ of the T-tubules. We find that halving this grid spacing does not change the solutions to the system. (For the simulations below in which L and δ are decreased below their physiological values, we decrease Δx proportionally so that it remains equal to $\delta/2$.) Given the selected values of Δx, Δt, D_c, and D_{sr}, it is apparent that a fully explicit solution method would have been adequate, but we retain the semi-implicit scheme because the cost is negligible.

In our simulations of the full system, we eliminate transient effects by initializing the system with the steady-state solution of the spatially uniform system (obtained by solving the steady state forms of (6)–(10) with $g \equiv 1$), and then simulating for several seconds or until $\|d \ln u/dt\|_\infty < 2 \times 10^{-2}\ s^{-1}$, whichever comes first. We find this is sufficient to bring the system to its resting behavior (steady state or oscillations, depending on $[Ca^{2+}]_e$).

4.2. ***SR channel dynamics.*** The model's steady-state channel open probability (P_o) is a bell-shaped function of cytoplasmic Ca^{2+} levels. This is shown in Fig. 2. The peak is at $[Ca^{2+}]_i = 1.5\ \mu$M, which is within the experimental range of $\sim$1–10 μM (Fabiato, 1985). The peak open probability is 0.07, which is close to

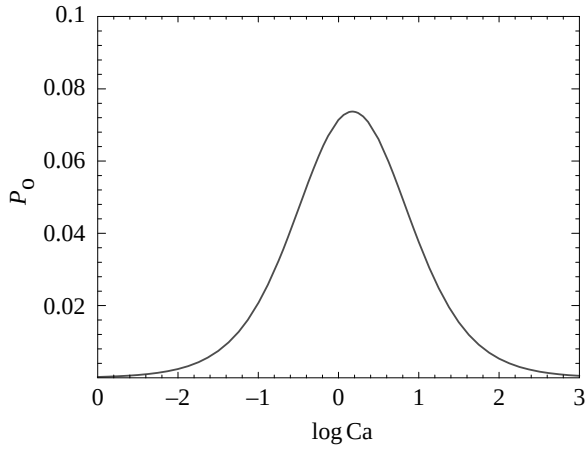

Figure 2. The steady-state channel open probability (P_o) as a function of $[Ca^{2+}]_i$ (in units of $\log_{10}$ μM). The peak open probability is 0.07, close to the steady-state open probability of $\sim$0.1 attained in experiment for the $[Ca^{2+}]_i$ level, thought to maximally activate the channels [Valdivia *et al.* (1995), Fig. 2D, curve c].

the steady state open probability of $\sim$0.1 found experimentally for the $[Ca^{2+}]_i$ level thought to maximally activate the channels [Valdivia *et al.* (1995), Fig. 2D, curve c].

It has been suggested (Valdivia *et al.*, 1995) that channels are most fully activated in the 10 μM range, a $[Ca^{2+}]_i$ level higher than the bulk $[Ca^{2+}]_i$ attained during contraction. The putative explanation for this discrepancy is that, due to spatial effects, $[Ca^{2+}]_i$ in the microdomains adjacent to the L-type and RyRs reaches a higher level during excitation than does bulk $[Ca^{2+}]_i$. The nonuniform longitudinal distribution of channels in the present model does result in higher $[Ca^{2+}]_i$ at T-tubule locations than between T-tubules (see below). However, this difference is not sufficient to allow a parameter set which yields both a higher peak $[Ca^{2+}]_i$ for the RyRs and faithful reproduction of the bulk $[Ca^{2+}]_i$ dynamics. To be more physiologically accurate, we could include in the model explicit microdomains from which the diffusion of Ca^{2+} was restricted. However, because our present purpose is simply to demonstrate the plausibility of a significant effect of heterogeneity on cardiac-calcium dynamics, we restrict ourselves to the given minimal model. In addition, since Ca^{2+} microdomains have not been well-defined, let alone quantitatively characterized, modeling of microdomains would not be physiologically meaningful at this time.

In addition to the steady-state response, the model also captures the correct dynamics of channel activation in response to excitation. Figure 3 shows the time course of changes in channel open fraction in response to step changes in cytoplasmic $[Ca^{2+}]$ from a resting level of 0.1 μM to levels of 0.5, 1, 1.5, 3, and 5 μM at times $t = 0.2$, 2, 3.5, 4.5, and 5.5 s, respectively. The time course exhibits the correct excitation and adaptation time scales ($\mathcal{O}(10)$ ms and $\mathcal{O}(100)$ ms, respectively)

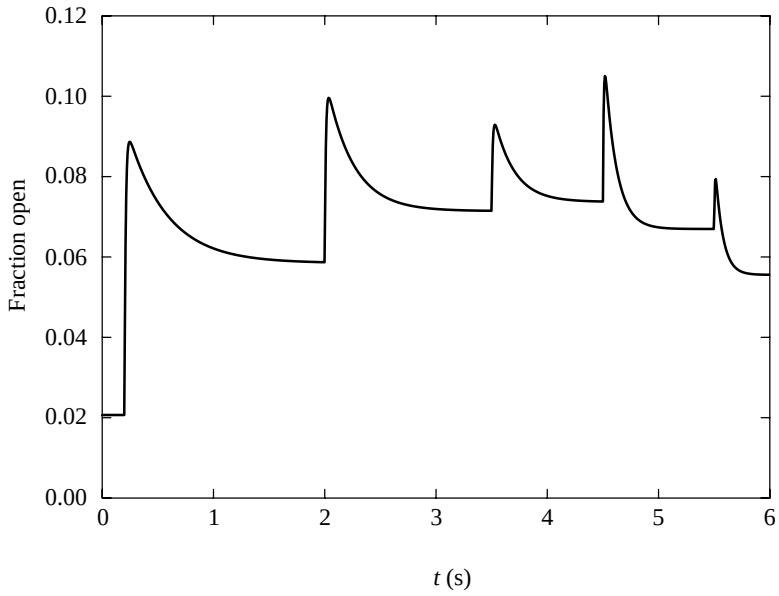

Figure 3. Numerical simulation of adaptation of channels to maintained stimuli. $[Ca^{2+}]_i$ is raised in successive steps from 0.1 μM to 0.5, 1, 1.5, 3, and 5 μM at times $t = 0.2$, 2, 3.5, 4.5, and 5.5 s, respectively. The time course exhibits the correct excitation and adaptation time scales ($\mathcal{O}(10)$ ms and $\mathcal{O}(100)$ ms, respectively) for the step up to $[Ca^{2+}]_i = 1$ μM, in agreement with the findings of Valdivia *et al.* (1995).

for the step up to $[Ca^{2+}]_i = 1$ μM, in agreement with the findings of Valdivia *et al.* (1995). Adaptation time decreases with the $[Ca^{2+}]_i$ level.

4.3. ***Resting behavior.*** In this, and the following section, we consider the steady-state and transient dynamics within a single sarcomere. At physiological $[Ca^{2+}]_e$ (1 mM), the system displays a steady-state $[Ca^{2+}]_i$ profile which varies significantly over the length of a sarcomere. Figure 4 shows the resting $[Ca^{2+}]_i$ distribution over one sarcomere length for $L = 2$ μm, which is approximately the physiological T-tubule periodicity, as well as for periodicities of 1, 1.33, 1.35, 1.37, 1.41, 1.5, and 1.67 μm (using the same distribution shape $g(x)$ given in (11)), and for the spatially uniform version of the system. We have included the distributions for the shorter nonphysiological values of L to demonstrate that the $[Ca^{2+}]_i$ distribution is particularly sensitive to this parameter near $L = 1.35$ μm. As we shall see in Section 4.6, this value will turn out to be a 'bifurcation' point for traveling-wave propagation; waves will propagate for reaction term periodicities smaller than this value and will be blocked for larger periodicities. Of course, we could also interpret this result in terms of the diffusion coefficients, since the nondimensionalized version of equations (9) and (10) only contains L in combination with the diffusion coefficients.

When the channel distribution is spatially uniform, resting $[Ca^{2+}]_i$ is also distributed spatially uniformly, with a concentration of 0.1 μM. For the short T-tubule

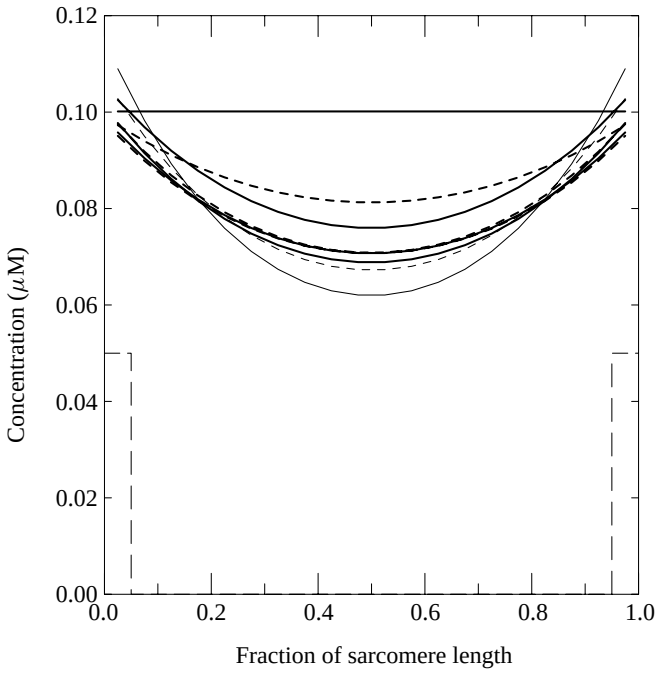

Figure 4. The resting distribution of $[Ca^{2+}]_i$ over one dimensionless sarcomere length for sarcomere lengths of 0 (which corresponds to uniformly-distributed RyRs), 1, 1.33, 1.35, 1.37, 1.41, 1.5, 1.67, and 2 μm (approximately the physiological value), in order of decreasing minimum value. The shape of the distribution is particularly sensitive to sarcomere length at lengths near 1.35 μm. Weighting of RyRs and SL transport terms (long dashes) is nonuniform for all but the first curve. Maximum of the weighting is 10. The horizontal axis represents the fractional longitudinal distance along a sarcomere.

distribution period $L = 1$ μm, resting $[Ca^{2+}]_i$ is at approximately the same level near the T-tubules as it is in the spatially uniform case. Between the T-tubules, it drops to a slightly lower value. As L is progressively increased, the inter-T-tubule drop in resting $[Ca^{2+}]_i$ increases as well. When L takes on its physiological value of 2 μm, resting $[Ca^{2+}]_i$ at the midpoint between T-tubules is at about 60% of its level at the T-tubules. This can be understood as follows.

The most significant calcium release sites are the RyRs, and high calcium concentration close these channels (cf. Fig. 2). Since the RyRs are localized at the T-tubules, whereas the SR pumps that remove cytosolic calcium are distributed in space, it is apparent why the resting $[Ca^{2+}]_i$ will be somewhat lower between T-tubules than at T-tubule locations. If the diffusion time scale is significantly shorter than the reaction time scale this difference will not be large. If the time scale of the reaction terms is of the same order or shorter than that of diffusion, the effect of diffusion will be weaker, and resting $[Ca^{2+}]_i$ will drop significantly between T-tubules. As sarcomere length increases, so does the time scale of diffusion across a sarcomere, and thus the drop in steady-state $[Ca^{2+}]_i$ increases as well.

We can obtain a more precise estimate of the ratio of the two time scales in the present model as follows. The time scale for diffusion across one sarcomere is $\tau_{d=}L^2/D_c = 4\ \mu\text{m}^2/400\ \mu\text{m}^2\ \text{s}^{-1} = 10$ ms. This should be compared to the time scales at steady state of the most significant Ca^{2+}-handling processes, the SR channels and pumps. These time scales, τ_{ch} and τ_p, respectively, are the reciprocals of the corresponding rate process divided by $[Ca^{2+}]_i$,

$$\tau_{ch} \equiv \left(\frac{vr \cdot ch \cdot u_2(u_5 - u_4)}{u_4} \right)^{-1} \tag{12}$$

$$\tau_p \equiv \left(\frac{vr \cdot p_1 u_4}{(u_4^2 + p_2^2)} \right)^{-1}. \tag{13}$$

If we use the resting values $u_4 = 0.1\ \mu$M, $u_5 = 1$ mm, and $u_2 = L_2 u_4/[u_4^2 + (L_1 + L_2)u_4 + L_1 L_2]$ (Tang and Othmer, 1994a) (where $L_1 \equiv l_{-1}/l_1$ and $L_2 \equiv l_{-2}/l_2$) in these equations, we find that the resulting time scales for the channels and pumps are both approximately 1.4 ms, which is very close to the value $\tau_r = 1.3$ ms estimated earlier (cf. Table 1). Thus $\theta \sim 7$, i.e., the time scale for diffusion is about 7 times that for calcium handling.

The Ca^{2+}-handling processes located at the T-tubules — all of the significant ones except for the SR pumps — see approximately the same local resting $[Ca^{2+}]_i$ in all of the above cases. However, the spatial average resting $[Ca^{2+}]_i$ is lowered as L is increased to its physiological value, because less Ca^{2+} is available at rest to be pumped into the SR, which leads to less Ca^{2+} flux through those channels that are open. As a consequence, the average resting $[Ca^{2+}]_{sr}$ is reduced, and for physiological L is at only 2/3 of its level in the spatially uniform case. This is illustrated in Fig. 5, where it is seen that the mean of the distribution is particularly sensitive to sarcomere length at lengths near 1.35 μm. There may in fact be a hysteresis loop in the response, but this will not be pursued here.

4.4. ***Excitability, graded response, and oscillations.*** We now consider the time-dependent behavior of the full model by simulating its response to stimuli applied simultaneously at all T-tubule locations throughout the length of a cell. (In practice we simulate a section of one sarcomere length L using periodic boundary conditions.) Figures 6 and 7 illustrate the response of the model to a 50 ms influx of Ca^{2+} through the L-type channels at various fluxes. $[Ca^{2+}]_e$ has the physiological value of 1 mM during these simulations, and so resting $[Ca^{2+}]_i$ initially has the baseline distribution (in the $\sim$0.1 μM range) described above in Section 4.3.

Figure 6 shows the spatial distribution of $[Ca^{2+}]_i$ over one sarcomere in response to fluxes of spatial average rates 70 and 80 μM s^{-1}. The lower flux elicits a weak response, $[Ca^{2+}]_i$ does not rise much above baseline, and the response exhibits significant spatial variation over the length of a sarcomere. The higher flux used

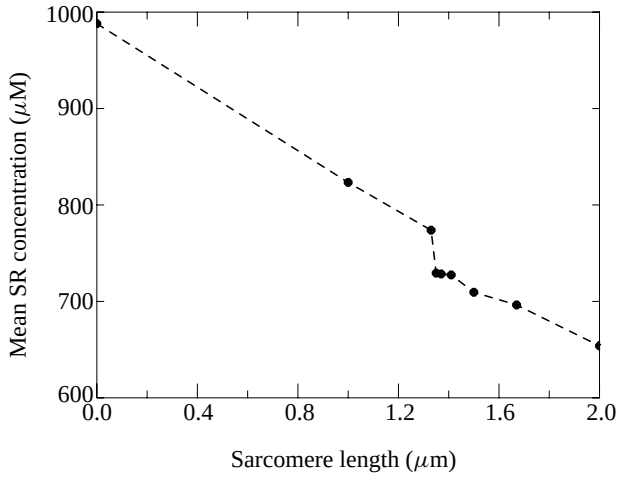

Figure 5. The mean steady state $[Ca^{2+}]_{sr}$ as a function of the sarcomere length.

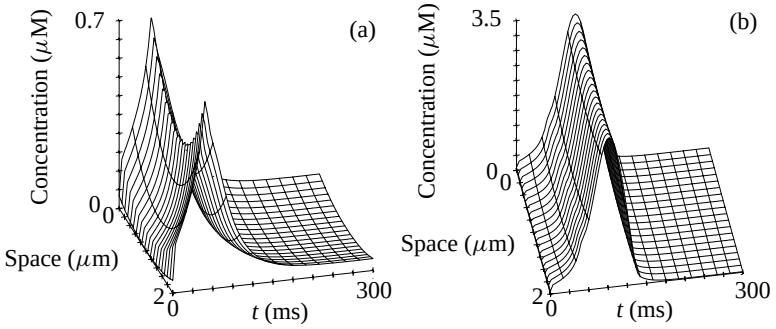

Figure 6. Response of the model to a subthreshold (a) and superthreshold (b) Ca^{2+} stimulus. In (a) a Ca^{2+} influx of spatial average rate 70 μM s^{-1} was applied for 50 ms at the T-tubule locations. In (b) the stimulus is 80 μM s^{-1} for the same duration. Shown is the $[Ca^{2+}]_i$ distribution over the length of one sarcomere (2 μm) for a period of 300 ms following onset of stimulation. The endpoints of the domain are at the midpoints of adjacent T-tubules. In (a) the response exhibits significant spatial variation over the length of a sarcomere, while in (b) it is essentially uniform in space.

in Fig. 6(b) elicits a significant excitation response, in which $[Ca^{2+}]_i$ rises into the micromolar range before returning to baseline. This superthreshold response exhibits little spatial variation over the length of a sarcomere.

In Fig. 7 we compare the responses to fluxes of various rates. For the lower rates used in the simulations of Fig. 7(a), the response does not involve a significant departure of $[Ca^{2+}]_i$ from baseline, while for the higher rates of Fig. 7(b), there is a significant excitation response. There is a threshold rate of around 73 μM s^{-1} which separates these two response patterns. The system thus exhibits excitability. In both panels the magnitude of the response increases with the flux, and thus the system exhibits graded response as well.

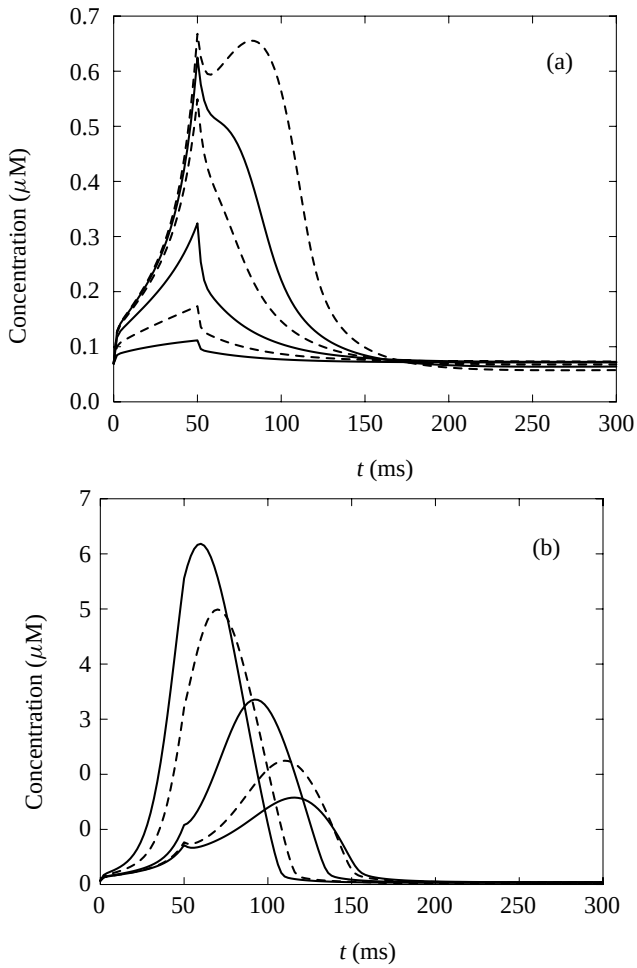

Figure 7. Graded sub- and superthreshold responses to pulse Ca^{2+} stimuli applied for $0 < t < 50$ ms at the T-tubule locations. In (a) the spatial average fluxes are 20, 40, 60, 70, 72, and 73 μM s^{-1}, and in (b) they are 74, 75, 80, 100, and 120 μM s^{-1}, both in order of increasing response magnitude. The responses are measured at a longitudinal location midway between the center of a T-tubule and the midpoint between T-tubules, in order to reflect the spatial average response.

The maximum $[Ca^{2+}]_i$ attained during the excitation responses to the larger fluxes used in Fig. 7(b) are higher than experimentally derived estimates [0.5–3 μM (Bers, 1991b)] of the maximum attained during contraction. In addition, the time scale of Ca^{2+} removal in the model ($\sim$50 ms) is faster than time scales [a few hundred ms (Beuckelmann and Wier, 1988)] found experimentally. The latter discrepancy is due to the low K_m of the SR pump (see Table 2), which causes the pump's Ca^{2+} removal rate to reach its maximum at low $[Ca^{2+}]_i$ — and thus early in the excitation response — resulting in a high average Ca^{2+} removal rate during the course of excitation and thus a short time scale for removal. The reason

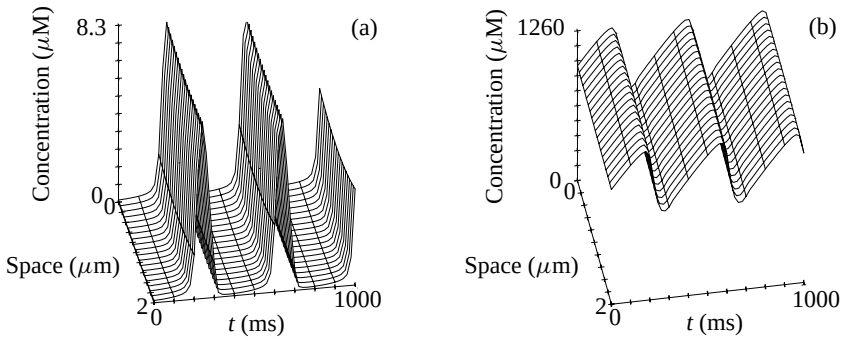

Figure 8. The system becomes self-oscillatory when external $[Ca^{2+}]$ is raised sufficiently, in this case to 10 mM. Shown is the $[Ca^{2+}]_i$ distribution (a) and $[Ca^{2+}]_{sr}$ distribution (b) over the length of one sarcomere (2 μm) for a period of 1 s. The endpoints of the domain are at the midpoints of adjacent T-tubules. The oscillations exhibit little spatial variation over the length of a sarcomere.

for the elevated maximum $[Ca^{2+}]_i$ is not clear, but presumably the pump's low K_m somewhat elevates its resting Ca^{2+} removal rate, requiring parameter choices which elevate the rate of the balancing process, SR channel flux, which in turn yields an elevated excitation response. Explicit modeling of Ca^{2+} microdomains could eliminate the discrepancy in Ca^{2+} removal rate (and therefore presumably the discrepancy in maximum $[Ca^{2+}]_i$ response as well) by allowing the RyRs to see a higher $[Ca^{2+}]_i$ during excitation than do the pumps. This would allow the RyRs to be maximally open at a $[Ca^{2+}]_i$ level higher than the bulk $[Ca^{2+}]_i$ attained during contraction (Valdivia *et al.*, 1995), which would permit the pump's K_m to be raised while still remaining below the channels' peak open $[Ca^{2+}]_i$ level. This last property is necessary for the system to be 'excitable', by which we mean that for a $[Ca^{2+}]_i$ stimulus above a certain threshold level, the SR must release enough Ca^{2+} so that $[Ca^{2+}]_i$ rises significantly above this threshold before returning to its resting level.

When $[Ca^{2+}]_e$ is raised sufficiently, the system exhibits spontaneous oscillations in $[Ca^{2+}]_i$ (Fig. 8), as does the experimental system (Wier and Blatter, 1991b). The oscillations in the model exhibit little spatial variation over the length of a sarcomere. Numerical experimentation reveals that the threshold $[Ca^{2+}]_e$ for onset of oscillations is slightly above 3 mM, approximately the threshold level for onset of oscillations reported from experiment (Stern *et al.*, 1988). If the Ca^{2+}-handling processes are instead distributed uniformly, we find, from numerical spectral analysis of the Jacobian of the system's reaction terms, that the threshold is 1.55 mM, about half the threshold for the physiological distribution. Heterogeneity may thus serve to prevent spontaneous oscillations in a resting myocyte. In the model, $[Ca^{2+}]_{sr}$ also oscillates, but without departing significantly from the 1 mM level it maintains at rest under physiological $[Ca^{2+}]_e$ [Fig. 8(b)]. Thus, as was found in Tang and Othmer (1994a), overload of the SR is not necessary for spontaneous oscillations.

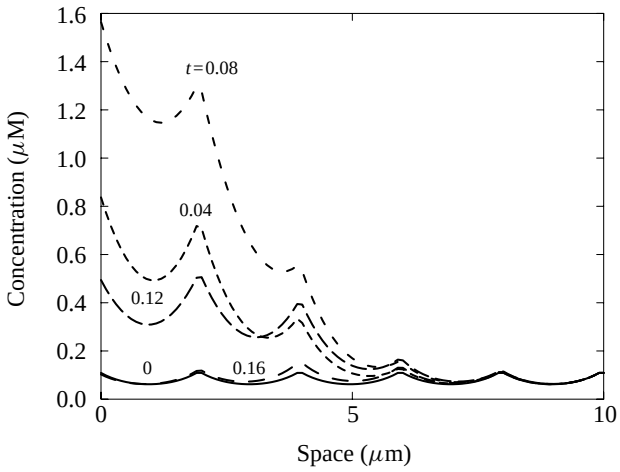

Figure 9. Localized response of the system to a local stimulus. A Ca^{2+} influx of 80 μM s^{-1} was applied at the leftmost 4 μm of the cell for $0 < t < 50$ ms. $[Ca^{2+}]_i$ is shown at the times indicated, for the first 10 μm of a 100 μm cell, which is approximately the length of a cardiac myocyte (Jaffe, 1993). The cell is quiescent at $t = 0$ and again at $t = 0.16$ s, and the disturbance does not spread beyond 10 μm.

4.5. ***Wave propagation.*** For physiological $[Ca^{2+}]_e$, the model is incapable of propagating a traveling wave of elevated $[Ca^{2+}]_i$ in response to locally applied stimuli, even though it is capable of a robust excitation response to moderate stimuli applied simultaneously at all T-tubule locations throughout the length of a cell. Figure 9 shows the time course of $[Ca^{2+}]_i$ over the first 10 microns of one cell length following a 50 ms influx of Ca^{2+} through the L-type channels located in the leftmost 4 μm of the cell. The flux is 80 μM s^{-1}, a rate which elicits the significant excitation response seen in Fig. 6(b) when the stimulus is applied at every T-tubule. The response to the locally-applied stimulus is a locally-elevated $[Ca^{2+}]_i$ signal which does not propagate far. Even a much larger flux of 800 μM s^{-1} elicits only a nonpropagating local response (Fig. 10), despite the fact that $[Ca^{2+}]_i$ near the point of stimulation attains values significantly above the maxima of the excitation responses of Fig. 7(b).

When $[Ca^{2+}]_e$ is raised to 3 mM, just below the oscillation threshold, the system does propagate a wave in response to the same moderate stimulus protocol used in Fig. 9, as is shown in Fig. 11. The model thus reproduces the finding (Cheng *et al.*, 1996a) that cardiac myocytes are capable of propagating Ca^{2+} waves at elevated $[Ca^{2+}]_e$ but not under normal conditions. The wave speed in the figure is about 170–180 μm s^{-1}, which is somewhat faster than the experimental value of 116 ± 31 μm s^{-1} (Jaffe, 1993).

Waves have been found experimentally at $[Ca^{2+}]_e = 10$ mM (Cheng *et al.*, 1996a), a concentration at which the model exhibits spontaneous oscillations. Because it is oscillatory at this $[Ca^{2+}]_e$ level, we find that there are no traveling waves of

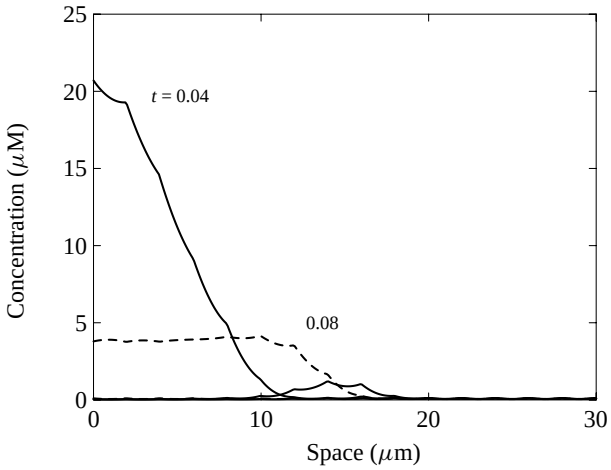

Figure 10. The response remains localized even to very large local stimuli. A Ca^{2+} influx of 800 μM s^{-1} was applied at the leftmost 4 μm of the cell for $0 < t < 50$ ms. The cell is quiescent at $t = 0$ and again at $t = 0.16$ s.

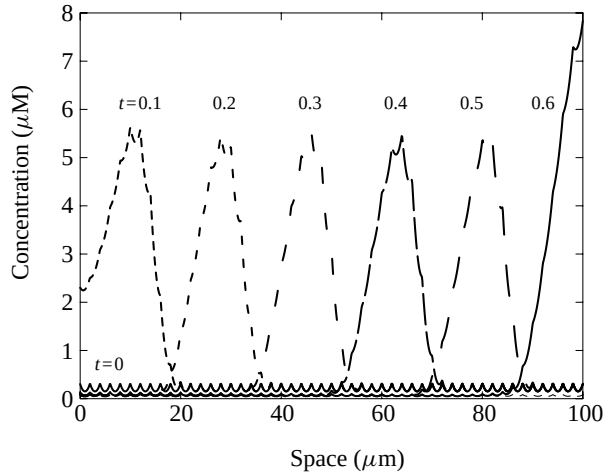

Figure 11. At somewhat elevated $[Ca^{2+}]_e$ (3 mM), a moderate local stimulus generates a propagating wave of elevated $[Ca^{2+}]_i$. A Ca^{2+} influx of 80 μM s^{-1} was applied at the leftmost 4 μm of the cell for $0 < t < 50$ ms. The cell is quiescent at $t = 0$ and again at $t = 0.7$ s.

permanent form: a localized stimulus only propagates for a finite distance, until the $[Ca^{2+}]_i$ oscillation reaches its peak and absorbs the propagating signal. Nevertheless, as is illustrated in Fig. 12, a signal can still propagate across a significant fraction of the cell length. To more accurately reproduce the results of Cheng *et al.* (1996a), the model should be in the excitatory regime at this $[Ca^{2+}]_e$ level. We note, however, that for the same species (rat), the threshold for onset of oscillations has been reported elsewhere (Stern *et al.*, 1988) to be about 3 mM, consistent with the

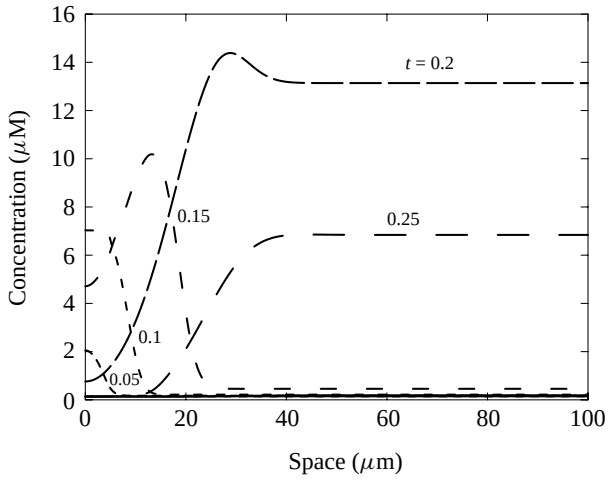

Figure 12. At elevated $[Ca^{2+}]_e$ (10 mM) a moderate local stimulus generates a spatial signal of elevated $[Ca^{2+}]_i$ which propagates until the $[Ca^{2+}]_i$ oscillation reaches its peak and absorbs the propagating signal. A Ca^{2+} influx of 80 μM s^{-1} was applied at the leftmost 4 μm of the cell for $0 < t < 50$ ms. The cell is quiescent (at the low point of the oscillation) at $t = 0$ and again at $t = 0.3$ s.

behavior of the model. We are unable to find a reasonable parameter set which yields excitability at $[Ca^{2+}]_e = 10$ mM. As discussed above for several other properties, this could presumably be rectified by explicit modeling of microdomains. Inclusion of microdomains would allow extension of the range of $[Ca^{2+}]_i$, and therefore of $[Ca^{2+}]_e$, over which the system exhibits excitability.

4.6. ***The effect of heterogeneity.*** We now examine the role played by channel distribution on the wave propagation properties of the system. We do so by progressively decreasing the period L of the T-tubule distribution, as was done for steady-state distributions in Section 4.3, and applying the same local stimulus as in Fig. 9. Figure 13 depicts the response when $L = 1.35$ μm, for which the local signal now elicits a larger response which propagates for a significant distance, but which dies well before it reaches the far end of the cell. Figure 14 shows the response for $L = 1.33$ μm. At this shorter T-tubule spacing, the system propagates a robust traveling wave whose speed is speed 110–120 μm s^{-1}. Finally, in Fig. 15, we show the response of the system with all calcium handling mechanisms distributed uniformly in space. This system propagates a traveling wave with a speed of 200 μm s^{-1}. Thus, there is a threshold spacing of around 1.35 μm, below which waves propagate and above which they do not. As noted in Section 4.3, the shape of the resting distribution of $[Ca^{2+}]_i$ is particularly sensitive to L near this bifurcation value.

The spatial distribution of Ca^{2+} channels and other Ca^{2+}-handling processes thus plays a crucial role in determining whether traveling waves can propagate. The reason for this effect is not immediately apparent, since the spatial scale of the

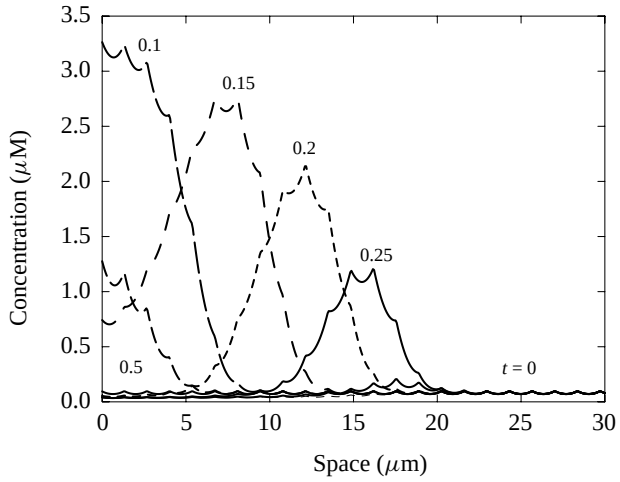

Figure 13. A moderate reduction in the spacing between T-tubules to 1.35 μm results in a dying wave in response to a moderate local stimulus. A Ca^{2+} influx of 80 μM s^{-1} was applied at the leftmost 4 μm of the cell for $0 < t < 50$ ms. The cell is quiescent at $t = 0$ and again at $t = 0.35$ s.

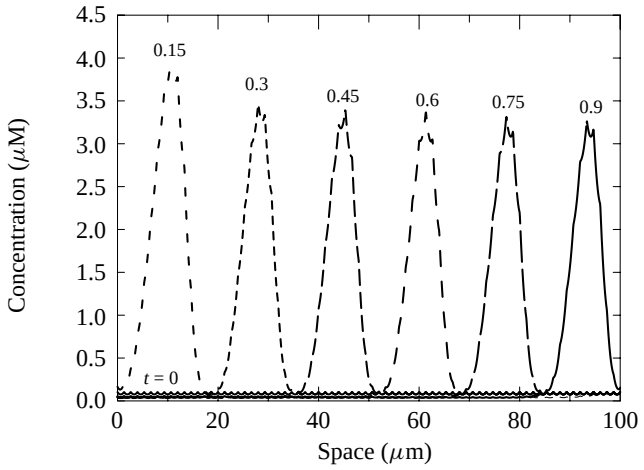

Figure 14. Sufficiently short spacing between T-tubules (1.33 μm) results in a robust traveling-wave response to the stimulus used in Fig. 13. The cell is quiescent at $t = 0$ and again at $t = 1.0$ s.

nonpropagating Ca^{2+} transient of the physiological distribution (Figs 9 and 10) is considerably larger than the period L of the heterogeneity. Thus, it is not the case that Ca^{2+} released from one channel cluster simply fails to diffuse to the locations of adjacent clusters at significant levels. The explanation for wave blocking must instead be that heterogeneity alters some effective parameter of the system.

To understand the cause of wave blocking, we consider the resting distribution of $[Ca^{2+}]$ discussed in Section 4.3. Because the physiological pattern of heterogeneity

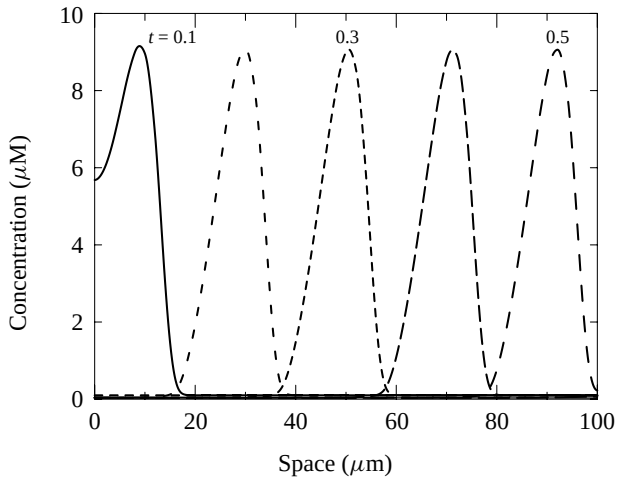

Figure 15. Uniform distribution of all Ca^{2+}-handling processes results in a robust traveling-wave response to the stimulus used in Fig. 13. The cell is quiescent at $t = 0$ and again at $t = 0.6$ s.

lowers resting $[Ca^{2+}]_{sr}$ to 2/3 of its level in the spatially uniform case, the Ca^{2+} flux through the SR channels is reduced proportionally. As a result, stimuli elicit a weaker excitation response in the case of the heterogeneous distribution, a response too weak to allow wave propagation. Since the shape of the resting distribution of $[Ca^{2+}]_i$ is particularly sensitive to L at the bifurcation point for wave blocking $L = 1.35$ μm, resting $[Ca^{2+}]_{sr}$ drops sharply with increasing L near this point, resulting in a sharp weakening of the channel flux.

We have confirmed this explanation by varying the channel flux. To compensate for the lowering of resting $[Ca^{2+}]_{sr}$ in the heterogeneous case, we increase the SR channel conductance *ch* by 50% wherever $[Ca^{2+}]_i$ rises above a threshold of 0.15 μM outside the stimulated region. The threshold is just above the maximum value of resting $[Ca^{2+}]_i$. This gives the system a channel flux equal to that of the spatially uniform case in response to excitatory stimuli, while retaining the system's resting properties and its local response to the standard stimulus. Figure 16 shows the response of this altered system to the same moderate stimulus protocol used in Fig. 9. In this case the system now readily propagates a traveling wave. Conversely, decreasing *ch* by 1/3 wherever $[Ca^{2+}]_i$ rises above threshold outside of the stimulated region causes wave blocking in the spatially uniform system, even for very large local stimuli (Fig. 17).

5. DISCUSSION

We have developed a minimal model of cardiac-calcium dynamics, incorporating physiological distributions of Ca^{2+}-handling processes and physiologically-

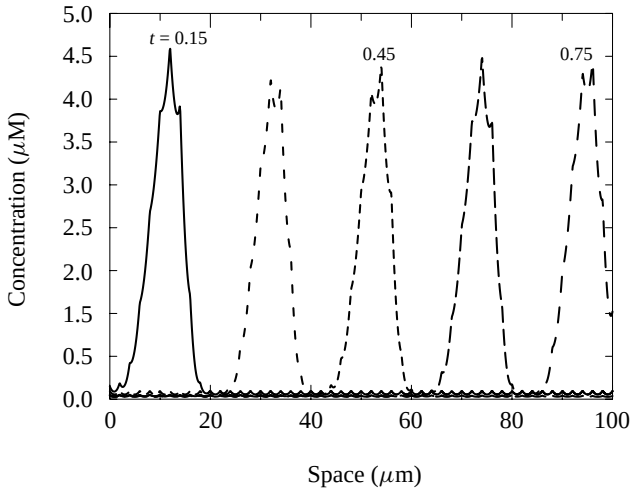

Figure 16. Elevating the SR Ca^{2+} flux during excitation to that of the spatially uniform system restores the traveling-wave response to a moderate local stimulus. The channel conductance (*ch*) was increased by 50% wherever $[Ca^{2+}]_i$ exceeded a threshold of 0.15 μM outside of the stimulated region.

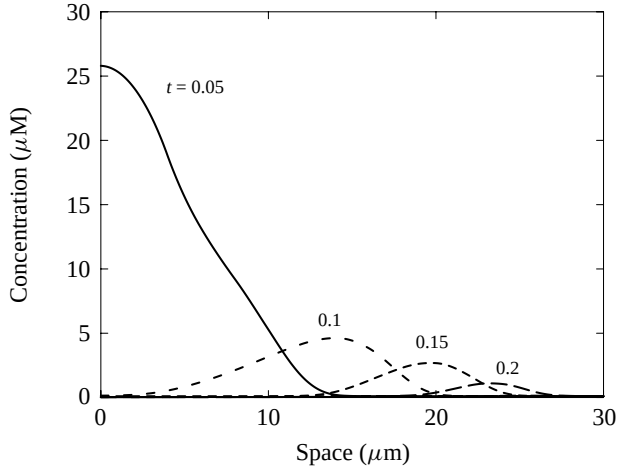

Figure 17. Reducing the SR Ca^{2+} flux of the spatially uniform system during excitation to that of the system with physiological distribution restores the localized response, even to a very large local stimulus. A Ca^{2+} influx of 800 μM s^{-1} was applied at the leftmost 4 μm of the cell for $0 < t < 50$ ms. Channel conductance (*ch*) was decreased by 1/3 wherever $[Ca^{2+}]_i$ exceeded a threshold of 0.15 μM outside of the stimulated region.

reasonable parameter values, which reproduces a variety of experimentally observed features. These include a bell-shaped channel open probability function, correct time scales for channel excitation and adaptation, correct resting $[Ca^{2+}]$ levels, excitability, graded response, spontaneous oscillations under perturbed conditons, wave blocking at physiological $[Ca^{2+}]_e$, and wave propagation at high $[Ca^{2+}]_e$. The time scales of the model's Ca^{2+}-handling processes are not slow compared to that

of diffusion, and as a result, heterogeneity exerts a significant effect on the system's behavior, consistent with the theory developed in Spiro (1997).

The significant finding for the present model is that there are physiologically-reasonable parameter sets for which it is the heterogeneity in the physiological distribution of Ca^{2+}-handling processes which prevents propagation of traveling waves. A spatially uniform distribution allows waves to propagate robustly for the same parameter set. With heterogeneity present, our parameter set lies near a bifurcation point for traveling-wave blocking, so that a moderate change in a parameter, such as a rise in external $[Ca^{2+}]$ can move the system from a wave-blocking to a wave-propagating regime. This provides an attractive explanation for wave blocking under physiological conditions in cardiac myocytes (Cheng *et al.*, 1996a), as well as for the physiological spacing of Ca^{2+}-handling processes and sarcomere length. Others have modeled the effects of nonuniform channel spacing, either using random-located sites for IP_3-mediated release (Bugrim *et al.*, 1997), or in cardiac myocytes, using highly-simplified models of channel dynamics (Keizer *et al.*, 1998; Keizer and Smith, 1998). The latter authors find that the speed of the Ca^{2+} waves is linearly related to the diffusion coefficient over a four-fold variation of the diffusion coefficient, rather than with the square-root dependence frequently found in theoretical models. Others have also shown that the square-root dependence of speed on the diffusion coefficent is not universally true in excitable systems (Othmer and Schaap, 1998).

Alternative explanations for wave blocking have drawbacks which the proposed explanation does not. A very simple alternative mathematical explanation for wave blocking can be given by analogy to the equal area condition for wave propagation in a single-variable reaction–diffusion system,

$$u_t = Du_{xx} + f(u). \tag{14}$$

If $f(u)$ has negative area, then waves of excitation will not propagate, and conversely. Although calcium dynamics are more accurately modeled using multiple state variables, if we assume that normal calcium dynamics are a higher-dimensional analog of the case where f has negative area and that raising external Ca^{2+} is analogous to altering a reaction-term parameter so that the area under f becomes positive, then wave blocking might be explained by a higher dimensional analog of the equal area condition. However, a drawback of such an explanation is that the negative area requirement imposes constraints on the form of f under normal conditions, and these constraints may preclude an optimal contraction response, for example by effectively weakening the response.

A second explanation for wave blocking might involve an effect of external calcium on the magnitude of potential wave-triggering events. According to this explanation, the system is capable of wave propagation under all external calcium regimes, but under normal conditions events capable of triggering a wave seldom occur. In cardiac myocytes, spontaneous calcium releases from the SR are in

fact more frequent and of larger magnitude when external calcium is raised (Cheng *et al.*, 1996a). However, increasing the frequency of release (by application of ryanodine) under normal external calcium levels cannot elicit traveling waves (Cheng *et al.*, 1996a), suggesting that a wave-blocking mechanism other than control of triggering events may be at work.

A way around the drawbacks of these explanations is provided by our finding that sufficiently large gaps between channel clusters can stall an otherwise robust wave. Discretely distributed calcium release sites might allow a stronger f under normal conditions than does a spatially uniform distribution, while still precluding wave propagation.

In the present model, heterogeneity causes wave blocking by reducing mean resting $[Ca^{2+}]_i$ and thereby mean resting $[Ca^{2+}]_{sr}$, which results in an SR channel flux too weak to propagate a local stimulus. Alternative wave-blocking mechanisms are also plausible. For example, if Ca^{2+} transport across the SL is distributed uniformly rather than heterogeneously, we have found that mean resting $[Ca^{2+}]_i$ has approximately the same level as when SR channels are also distributed uniformly. However, as in the present form of the model, local resting $[Ca^{2+}]_i$ at the T-tubules is significantly higher than the mean $[Ca^{2+}]_i$. Ca^{2+} channels consequently see a higher resting $[Ca^{2+}]_i$ than in the case of uniform channel distribution, and so a larger fraction of them are open at steady state. This results in a leakier SR, which therefore again holds less Ca^{2+} at rest and so cannot release enough Ca^{2+} to propagate a local stimulus.

If heterogeneity is the cause of wave blocking in cardiac myocytes, the wave-blocking mechanism is likely to be somewhat different from either of the above two possibilities. This is because both of these mechanisms depend on the steady state distribution of $[Ca^{2+}]_i$, but in myocytes there is no steady state, since at rest there are spontaneous releases of Ca^{2+} from the channels. Nevertheless, the physiological wave-blocking mechanism may share the essential feature of these mechanisms, namely that a difference in the spatial distributions of opposing Ca^{2+}-handling processes (channels and pumps) results in significant local spatial variation in resting $[Ca^{2+}]$, and this variation causes some global property of the cell to differ significantly from the case when the opposing processes have identical distributions.

Whether or not there is a significant local spatial variation in resting $[Ca^{2+}]$ may be predicted, independently of the specific details of a heterogeneity-induced wave-blocking mechanism, from the magnitude of the ratio $\theta = \tau_d/\tau_r$ of the system's two spatial scales. If this ratio is small, the time scale of diffusion is much shorter than that of the heterogeneity, and so diffusion will greatly smooth out effects from local differences in Ca^{2+} sources and sinks. [See Spiro (1997) for a detailed analysis.] The resting state of the cell will thus closely approximate that of the spatially uniform case, and the same will be true of the system's dynamic behavior. On the other hand, if θ is not small, diffusion will not have a long range effect (on the spatial scale of the heterogeneity), and so the resting Ca^{2+} distribution may vary significantly in space. As a result, it is possible in this regime for a global

property of the system to be significantly altered by parameter changes which alter the resting distribution.

A second effect of heterogeneity is to approximately double the $[Ca^{2+}]_e$ threshold for onset of spontaneous oscillations in $[Ca^{2+}]_i$. Heterogeneity may thus serve to prevent spontaneous oscillations in a resting myocyte.

Whether or not heterogeneity is the cause of Ca^{2+} wave blocking or prevention of oscillations in real cells, the present results make it clear that very local (sub-sarcomere-scale) spatial variability in Ca^{2+} dynamics can have significant effects on the global behavior of the system. For an accurate understanding of Ca^{2+} dynamics, it may therefore be important for experimentalists to study cellular systems on this fine scale.

We have presented a minimal model of cardiac Ca^{2+} dynamics which exhibits significant effects due to heterogeneity. To more properly study these effects, a model incorporating more details of the physiology is desirable. Future extensions of this work should include a variety of additional features, such as Ca^{2+} buffering, Ca^{2+} handling by mitochondria, microdomains, and three-dimensional effects. However, the most important property to incorporate is stochastic release of Ca^{2+}. This is because the explanation for wave blocking presented here depends on the dynamics of Ca^{2+} at rest, and so to confirm this explanation with a more physiologically accurate model, a physiologically accurate description of resting Ca^{2+} dynamics is of primary importance. Resting Ca^{2+} dynamics are inherently stochastic in real cells.

REFERENCES

Allbritton, N. L. and T. Meyer (1993). Localized calcium spikes and propagating calcium waves. *Cell Calcium* **14**, 691–697.

Bell, J. (1990). Excitability behaviour of myelinated axon models, in *Reaction–Diffusion Equations*, K. J. Brown and A. A. Lacey (Eds), New York: Clarendon, pp. 95–116.

Berridge, M. J. (1993). Inositol trisphosphate and calcium signalling. *Nature* **361**, 315–325.

Bers, D. M. (1991a). *Excitation-Contraction Coupling and Cardiac Contractile Force*, Dordrecht: Kluwer.

Bers, D. M. (1991b). *Excitation-Contraction Coupling and Cardiac Contractile Force*, Norwell, MA: Kluwer.

Beuckelmann, D. and W. Wier (1988). Mechanism of release of calcium from sarcoplasmic reticulum of guinea-pig cardiac cells. *J. Physiol.* **405**, 233–255.

Bugrim, A. E., A. M. Zhabotinsky and I. R. Epstein (1997). Calcium waves in a model with a random spatially discrete distribution of Ca^{2+} release sites. *Biophys. J.* **73**, 2897.

Cannell, M. B., H. Cheng and W. J. Lederer (1994). Spatial nonuniformities in $[Ca^{2+}]_i$ during excitation-contraction coupling in cardiac myocytes. *Biophys. J.* **67**, 1942–1956.

Cheek, T. R., M. J. Berridge, R. B. Moreton and K. A. Stauderman (1994). Quantal Ca020+ mobilization by ryanodine receptors is due to all-or-none release from functionally discrete intracellular stores. *Biochem. J.* **301**, 879.

Cheng, H., W. J. Lederer and M. B. Cannell (1993a). Calcium sparks: elementary events underlying excitation-contraction coupling in heart muscle. *Science* **262**, 740–744.

Cheng, H., W. J. Lederer and M. B. Cannell (1993b). Calcium sparks: elementary events underlying excitation-contraction coupling in heart muscle. *Science* **262**, 740–744.

Cheng, H., M. Fill, H. Valdivia and W. J. Lederer (1995). Models of Ca^{2+} release channel adaptation. *Science* **267**, 2009–2010.

Cheng, H., M. R. Lederer, W. J. Lederer and M. B. Cannell (1996a). Calcium sparks and $[Ca^{2+}]_i$ waves in cardiac myocytes. *Am. J. Physiol.* **270**, C148–C159.

Cheng, H., M. R. Lederer, R.-P. Xiao, A. M. Gómez, Y.-Y. Zhou, B. Ziman, H. Spurgeon, E. G. Lakatta and W. J. Lederer (1996b). Excitation-contraction coupling in heart: new insights from Ca^{2+} sparks. *Cell Calcium* **20**, 129–140.

Dupont, G. and A. Goldbeter (1992). Oscillations and waves of cytosolic calcium: insights from theoretical models. *BioEssays* **14**, 485–493.

Dupont, G. and A. Goldbeter (1994). Properties of intracellular Ca^{2+} waves generated by a model based on Ca^{2+}-induced Ca^{2+} release. *Biophys. J.* **67**, 2191–2204.

Fabiato, A. (1985). Time and calcium dependence of activation and inactivation of calcium-induced release of calcium from the sarcoplasmic reticulum of a skinned canine cardiac Purkinje cell. *J. Gen. Physiol.* **85**, 247–289.

Fabiato, A. (1992). Two kinds of calcium-induced release of calcium from the sarcoplasmic recticulum of skinned cardiac cells, in *Excitation-Contraction Coupling in Skeletal, Cardiac, and Smooth Muscle*, New York: Plenum, pp. 245–263.

Fay, F. S. (1995). Calcium sparks in vascular smooth muscle: relaxation regulators. *Science* **270**, 588–589.

Gyorke, S. and M. Fill (1993). Ryanodine receptor adaptation: control mechanism of Ca^{2+}-induced Ca^{2+} release in heart. *Science* **260**, 807–809.

Hindmarsh, A. C. (1983). ODEPACK: a systematized collection of ODE solvers, in *Scientific Computing*, R. S. Stepleman (Ed.), Amsterdam: North-Holland, pp. 55–64.

Ikemoto, Noriaki, Antoniu, Bozena, Kang and Jaw-Jou (1992). Characterization of depolarization-induced calcium release from sarcoplasmic reticulum *in vitro* with the use of membrane potential probe. *Biochem. Biophys. Res. Comm.* **184**, 538–543.

Jaffe, L. F. (1993). Classes and mechanisms of calcium waves. *Cell Calcium* **14**, 736–745.

Katz, B. (1992). *Physiology of the Heart*, 2nd edn, New York: Raven Press.

Keizer, J. and L. Levine (1996). Ryanodine receptor adaptation and Ca^{2+}-Induced Ca^{2+} release-dependent Ca^{2+} oscillations. *Biophys. J.* **71**, 3477–3487.

Keizer, J., Y.-X. Li, S. Stojilkovic and J. Rinzel (1995). $InsP_3$-induced excitability of the endoplasmic reticulum. *Mol. Biol. Cell* **6**, 945–951.

Keizer, J. and G. D. Smith (1998). Spark-to-wave transition: saltatory transmission of calcium waves in cardiac myocytes. *Biophys. Chem.* **72**, 87

Keizer, J., G. D. Smith, S. Ponce-Dawson and J. Pearson (1998). Saltatory propagation of Ca^{2+} waves by Ca^{2+} sparks. *Biophys. J.* **75**, 595–600.

Laver, D. R. and G. D. Lamb (1998). Inactivation of Ca^{2+} release channels (ryanodine receptors RyR1 and RyR2) with rapid steps in $[Ca^{2+}]$ and voltage. *Biophys. J.* **74**, 2352–2364.

Li, Y.-X., J. Keizer, S. S. Stojilkovic and J. Rinzel (1995). Ca^{2+} excitability of the ER membrane: an explanation for IP_3-induced Ca^{2+} oscillations. *Am. J. Physiol.* **269**, C1079–C1092.

Lipp, P. and E. Niggli (1994). Modulation of Ca^{2+} release in cultured neonatal rat cardiac myocytes. *Circ. Res.* **74**, 979–990.

Lipp, P. and E. Niggli (1996). Submicroscopic calcium signals as fundamental events of excitation-contraction coupling in guinea-pig cardiac myocytes. *J. Physiol.* **492**, 31–38.

López-López, J. R., P. S. Shacklock, C. W. Balke and W. G. Wier (1994). Local, stochastic release of Ca^{2+} in voltage-clamped rat heart cells: visualization with confocal microscopy. *J. Physiol.* **480**, 21–29.

López-López, J. R., P. S. Shacklock, C. W. Balke and W. G. Wier (1995). Local calcium transients triggered by single L-type calcium channel currents in cardiac cells. *Science* **268**, 1042–1045.

Monck, J. R., I. M. Robinson, A. L. Escobar, J. L. Vergara and J. M. Fernandez (1994). Pulsed laser imaging of rapid Ca^{2+} gradients in excitable cells. *Biophys. J.* **67**, 505–514.

Nelson, M. T., H. Cheng, M. Rubart, L. F. Santana, A. D. Bonev, H. J. Knot and W. J. Lederer (1995). Relaxation of arterial smooth muscle by calcium sparks. *Science* **270**, 633–637.

Neu, J. C. and W. Krassowska (1993). Homogenization of syncytial tissues. *Crit. Rev. Biomed. Eng.* **21**, 137–199.

Niggli, E. and P. Lipp (1995). Subcellular features of calcium signalling in heart muscle: what do we learn? *Cardiovasc. Res.* **29**, 441–448.

Othmer, H. G. (1983). A continuum model for coupled cells. *J. Math. Biol.* **17**, 351–369.

Othmer, H. G. and P. Schaap (1998). Oscillatory cAMP Signaling in the Development of *Dictyostelium discoideum*. *Comments Theor. Biol.* **5**, 175–282.

Othmer, H. G. and Y. Tang (1993). Oscillations and waves in a model of IP_3-controlled calcium dynamics, in *Experimental and Theoretical Advances in Pattern Formation*, H. G. Othmer, P. K. Maini and J. D. Murray (Eds), New York: Plenum, pp. 277–313.

Parker, I., J. Choi and Y. Yao (1996b). Elementary events of $InsP_3$-induced Ca^{2+} liberation in *Xenopus* oocytes: hot spots, puffs and blips. *Cell Calcium* **20**, 105–121.

Parker, I. and I. Ivorra (1993). Confocal microfluorimetry of Ca^{2+} signals evoked in *Xenopus* oocytes by photoreleased inositol trisphosphate. *J. Physiol.* **461**, 133–165.

Parker, I. and Y. Yao (1991). Regenerative release of calcium from functionally discrete subcellular stores by inositol trisphosphate. *Proc. R. Soc. Lond.* **B241**, 269–274.

Parker, I. and Y. Yao (1995). Calcium puffs in *Xenopus* oocytes. *Ciba Symp.* **188**, 50–65.

Parker, I., W. J. Zang and W. G. Wier (1996a). Ca^{2+} sparks involving multiple Ca^{2+} release sites along Z-lines in rat heart cells. *J. Physiol.* **497**, 31–38.

Parys, J. B., L. Missiaen, H. D. Smedt, I. Sienaert and R. Casteels (1996). Mechanisms responsible for quantal Ca^{2+} release from inositol trisphosphate-sensitive calcium stores. *Pflügers Archiv: Eur. J. Physiol.* **432**, 359.

Peskoff, A., J. A. Post and G. A. Langer (1992). Sarcolemmal calcium binding sites in heart: II. Mathematical model for diffusion of calcium released from the sarcoplamic reticulum into the diadic region. *J. Membrane Biol.* **129**, 59–69.

Putney, J. W. Jr. and G. St. J. Bird (1993) The inositol phosphate-calcium signalling system in nonexcitable cells. *Endocrine Rev.* **14**, 610–631.

Rooney, T. A. and A. P. Thomas (1993). Intracellular calcium waves generated by $Ins(1, 4, 5)P_3$-dependent mechanisms. *Cell Calcium* **14**, 674–690.

Rousseau, E., J. S. Smith, J. S. Henderson and G. Meissner (1986). Single channel and $^{45}Ca^{2+}$ flux measurements of the cardiac sarcoplasmic reticulum calcium channel. *Biophys. J.* **50**, 1009–1014.

Sachs, F., F. Qin and P. Palade (1995). Models of Ca^{2+} release channel adaptation. *Science* **267**, 2010–2011.

Schiefer, A., G. Meissner and G. Isenberg (1995). Ca^{2+} activation and Ca^{2+} inactivation oc canine reconstituted cardiac sarcoplasmic reticulum Ca^{2+}-release channels. *J. Physiol.* **489**, 337–348.

Shacklock, P. S., W. G. Wier and C. W. Balke (1995). Local Ca^{2+} transients (Ca^{2+} sparks)

originate at transverse tubules in rat heart cells. *J. Physiol.* **487**, 601–608.
Shigesada, N., K. Kawasaki and E. Teramoto (1985). The speeds of traveling frontal waves in heterogeneous environments, in *Mathematical Topics in Population Biology, Morphogenesis, and Neurosciences: Proceedings of an International Symposium held in Kyoto, November 10–15, 1985*, E. Teramoto and M. Yamaguchi (Eds), Heidelberg: Springer-Verlag. Lecture Notes in Biomathematics **71**, 88–97.
Shigesada, N., K. Kawasaki and E. Teramoto (1986). Traveling periodic waves in heterogeneous environments. *Theor. Pop. Biol.* **30**, 143–160.
Spencer, C. I. and J. R. Berlin (1997). Calcium-induced release of strontium ions from the sarcoplasmic reticulum of rat cardiac ventricular myocytes. *J. Physiol.* **504**, 565–578.
Spiro, P.A. (1997). Mathematical studies of cell signal transduction, PhD thesis, University of Utah.
Stern, M. D. (1992). Theory of excitation-contraction coupling in cardiac muscle. *Biophys. J.* **63**, 497–517.
Stern, M. D., M. C. Capogrossi and E. G. Lakatta (1988). Spontaneous calcium release from the sarcoplasmic reticulum in myocardial cells: mechanisms and consequences. *Cell Calcium* **9**, 247–256.
Tanaka, H., T. Sekine, T. Kawanishi, R. Nakamura and K. Shigenobu (1998). Intrasarcomere [Ca^{2+}] gradients and their spatio-temporal relation to Ca^{2+} sparks in rat cardiomyocytes. *J. Physiol.* **508**, 145–152.
Tang, Y. and H. Othmer (1994a). A model of calcium dynamics in cardiac myocytes based on the kinetics of ryanodine-sensitive calcium channels. *Biophys. J.* **67**, 2223–2235.
Tang, Y. and H. G. Othmer (1994b). A model of calcium dynamics in cardiac myocytes based on the kinetics of ryanodine-sensitive calcium channels. *Biophys. J.* **67**, 2223–2235.
Tang, Y., J. Stephenson and H. Othmer (1996). Simplification and analysis of models of calcium dynamics based on IP-sensitive calcium channel kinetics. *Biophys. J.* **70**.
Taylor, C. W. (1994). Ca^{2+} sparks a wave of excitement. *TIPS* **15**, 271–274.
Tsugorka, A., E. Ríos, L. A. Blattner (1995). Imaging elementary events of calcium release in skeletal muscle cells. *Science* **269**, 1723–1726.
Valdivia, H., J. Kaplan, G. Ellis-Davies and J. Lederer (1995). Rapid adaptation of cardiac ryanodine receptors: modulation by Mg^{2+} and phosphorylation. *Science* **267**, 1997–2000.
Vélez, P., S. Györke, A. L. Escobar and M. Fill (1997). Adaptation of single cardiac ryanodine receptor channels. *Biophys. J.* **72**, 691–697.
Wier, W. G. and L. A. Blatter (1991a). Ca^{2+}-oscillations and Ca^{2+}-waves in mammalian cardiac and vascular smooth muscle cells. *Cell Calcium* **12**, 241–254.
Wier, W. G. and L. A. Blatter (1991b). Ca^{2+}-oscillations and Ca^{2+}-waves in mammalian cardiac and vascular smooth muscle cells. *Cell Calcium* **12**, 241–254.
Wier, W. G., J. R. López-López, P. S. Shacklock and C. W. Balke (1995). Calcium signalling in cardiac muscle cells. *Ciba Symp.* **188**, 146–164.
Williams, D. A. (1993). Mechanisms of calcium release and propagation in cardiac cells: do studies with confocal microscopy add to our understanding? *Cell Calcium* **14**, 724–735.
Xin, J. X. and J. Zhu (1995). Quenching and propagation of bistable reaction–diffusion fronts in multidimensional periodic media. *Physica* **D81**, 94–110.

Received 10 November 1998 and accepted 22 February 1999